Research Article

Nonlinear soil-pile interaction for wind turbines

Athanasios A. Markou*[1,2] and Amir M. Kaynia[1,3]

[1] *Norwegian Geotechnical Institute, NGI, Sognsveien 72, 0806 Oslo, Norway*
[2] *Department of Civil Engineering, Aristotle University of Thessaloniki, AUTH, Panepistimioupolis, 54124 Thessaloniki, Greece*
[3] *Department of Structural Engineering, Norwegian University of Science and Technology, NTNU, 7491 Trondheim, Norway*

Correspondence: *Corresponding author, Sognsveien 72, 0806 Oslo, Norway. Email: athanasios.markou@ngi.no

Present Address: Norwegian Geotechnical Institute (NGI), Sognsveien 72, 0806 Oslo, Norway

Summary

The current work presents a parametric study, which involves different generalized nonlinear mechanical formulations with different damping characteristics to account for the interaction between a monopile-supported offshore wind turbine and the surrounding soil. The novelty of the study lies in the fact that recently developed nonlinear mechanical models used so far for the simulation of high-damping rubber isolators, are introduced to describe the nonlinear hysteretic soil behavior. More specifically, the first generalized mechanical model consists of a combination of elastoplastic and trilinear elastic elements (labeled as model 3), while the second model consists of trilinear hysteretic models connected in parallel with trilinear elastic springs and hysteretic dampers used to ensure that the unloading stiffness will be as close as possible to the initial stiffness of the system (labeled as model 4). These newly-developed models are compared with well-known models within the industry, namely a model that comprises elastoplastic elements (labeled as model 1) and a model that comprises trilinear elastic springs (labeled as model 2). All these models provide exactly the same effective stiffness, but on the other hand different levels of damping are involved in each one of them. The goal of the present work is threefold, introducing novel mechanical models for the simulation of soil behavior, to investigate the effect of different soil damping levels in the response of offshore wind turbines and to highlight the limitations of the commonly-used models within the industry. To this end, the differences between the response due to different levels of damping characteristics and modeling approaches are shown, highlighting the importance of soil damping in the overall response of the system.

Keywords: Soil-pile interaction, Monopile, Trilinear hysteretic model, Plasticity, Non-linearity, Winkler's model, P-y curves

1 Introduction

Due to the fact that winds are stronger and steadier in the sea, offshore wind turbines (OWT) have attracted additional attention, (1). The most common type of wind turbine, is the horizontal axis wind turbine, which consists of: (i) the rotor, (ii) the drive train, (iii) the nacelle and the main frame, (iv) the tower, (v) the foundation, (vi) the machine controls and (vii) the balance of the electrical system (2). Furthermore, different types of wind turbine foundation exist: (i) monopile systems, (ii) tripod systems, (iii) jacket structures, (iv) suction caissons, (v) gravity-based foundations and (vi) floating systems, (3). Most of the OWT are currently supported on monopiles partly for economic reasons, (4).

The main dynamic excitation of OWT is caused by (i) the wind, (ii) the waves, (iii) the vibration due to imbalances of the rotor (1P) and (iv) the blade shadowing effect (2P/3P). The main sources of damping for OWT are (i) the aerodynamic, (ii) the structural, (iii) the nonlinear soil response, (iv) the hydrodynamic and (v) the radiation damping in soil, (3). In the case of OWT founded on monopile systems the natural frequencies of the overall system is more strongly affected by the soil-pile interaction, influencing the fatigue damage of the overall structure, (5).

Soil-pile interaction has been studied for decades, see (6–10). The most accurate way to simulate soil-pile interaction is to assume the soil as a continuum modeled analytically (e.g. (11)) or within the framework of the finite element method (12), (13). In practice however, most models are based on simple approaches. According to Pason and Kühn, (13), the most typical models for the simulation of monopiles include: (i) apparent fixity model, where a rigid connection is introduced at a certain depth below seabed, (ii) single element model, where the pile is assumed rigid and sets of springs and maybe dampers are introduced at its tips, and (iii) distributed element model, where a series of elements are introduced along the length of the pile and the elements can be either linear or non-linear systems with hysteretic damping with possible addition of viscous dampers. Among the three models, the last one is more appropriate to describe the behavior of the foundation of OWT due to the fact that the first two models under-predict the ultimate and fatigue loads.

Several researchers studied the effect of soil-monopile interaction of OWT. More specifically, Zaaijer (14) studied simplified dynamic modeling for monopiles by comparing the first and second bending modes of the foundation. The reference model for the monopile foundation was the Winkler distributed spring model (15), which was compared with three different models including (a) an apparent fixity model, (b) a model that represents the soil pile system with a stiffness matrix at the seabed level and (c) a model that represents the foundation with uncoupled springs for the possible degrees of freedom (DOF). The author concluded that the stiffness model outperforms the other two models. Along these lines Bush and Manuel (16) investigated the effect of extreme loading, using different models of monopile foundation. The fixed base model was compared with the apparent fixity model with a sufficient depth below mudline and a distributed element model, which includes linear elastic springs along the length of the monopile. The authors of the aforementioned study concluded that the long-term extreme loads for the apparent fixity and the distributed element model are larger compared to the fixed base model.

Klinkvort (17) simplified the elastoplastic model initially proposed by Boulanger et al (18) based on two components, one controlling loading and the other unloading. The model proposed by Klinkvort (17) is able to account for the behavior of the system due to gaps between the monopile and the ground. Taciroglu et al (19) proposed a model based on three components, namely leading-face element, rear-face element and drag-element. Schløer (20) used a similar model to investigate the response of OWT exposed to linear and nonlinear irregular waves, and highlighted the importance of the wave nonlinearity in the design of the OWTs.

Damgaard et al (21) used semi-analytical frequency-domain solutions to evaluate the dynamic impedance functions of the pile-soil system in order to calibrate a lumped mass model for integration into an aeroelastic multi-body code. They used three different models for the monopile foundation, namely the apparent fixity model, a fixed support model at the seabed level and a coupled lumped-parameter model. The authors of that study concluded that soil-pile interaction phenomena are important for the design in terms of fatigue at the seabed level. Similarly, Zania (22) followed the approach of Novak and Nogami (23) by employing the substructuring method (24) to deal with the dynamic soil-pile interaction for OWT systems. To this end, an iterative two-step analytical method based on analytical solutions was developed, which allowed for the consideration of the off diagonal terms of the dynamic impedances. The results showed the importance of the frequency dependent impedances and in particular of the cross coupling impedance terms on the eigenfrequencies and the damping of the system. Along similar lines, Ziegler et al (25) developed a frequency-domain method, where the soil was modeled with distributed linear springs, following the Winkler approach (15), in order to calculate wind-induced fatigue on monopile-supported OWT of large wind farms. The model was applied for sensitivity analysis and the results showed that water depth and wave period have important influence on fatigue loads.

Krathe and Kaynia (26) implemented in the aero-hydro-servo-elastic simulation tool FAST (27) a nonlinear macroelement foundation model for monopile at the pile head in terms of uncoupled generalized elastoplastic elements connected in parallel, initially proposed by Iwan (28). The authors of the aforementioned study highlighted that soil stiffness and damping should be considered as a part of the overall OWT simulation model, because they lead to natural frequencies closer to the frequencies of the environmental excitation. Along the same lines, Aasen et al (29) implemented a parametric study by using four different models for the simulation of the monopile foundation of OWT. More specifically, the first model comprises nonlinear elastic springs without the ability to dissipate energy, which is the common industry practice, the second one involved a linear elastic stiffness matrix ignoring energy dissipation, the third one was similar to the previous one with the addition of damping, while the last one involved a rigid massless beam, which at a specific depth is connected to the generalized model proposed by Iwan (28). The authors of that study pointed out that the current industry practice, namely the first model, is conservative for the estimation of the fatigue damage of the system and the last model, which reduces fatigue damage, is recommended.

Bisoi and Haldar (30) implemented an extensive dynamic study of OWT founded on a monopile, which was simulated by a beam on non-linear foundation Winkler model. The authors of that study used the finite element method for the simulations, whereas the largest part of the overall damping of the system came from the soil.

They concluded that the response of the overall system is affected by the interaction between the foundation and the superstructure, the soil nonlinearity, the rotor frequency and the magnitude of wave load. Carswell et al (31) investigated the effect of foundation damping of monopile-supported OWT on the first natural frequency under extreme storm loading. To this end, three different softwares were used, namely ADINA (32), INFIDEL (33) and FAST (27). The monopile foundation was simulated with a lumped parameter model, mounted at the base of a rigid link under the tower. The rigid link is used to represent the cross-coupling term in the pile stiffness. The conclusions from a stochastic load analysis was that foundation damping decreases the moment at the mudline level under extreme storm conditions.

Andersen et al (34) used a finite difference scheme to estimate the response of OWTs, where a simple Winkler model was calibrated against nonlinear p-y curves, with no ability of dissipating energy. The model was then simplified by replacing the monopile with an equivalent set of springs at mudline. The authors of the aforementioned study concluded that the reliability of the estimation of the first natural frequency of the system is a crucial measure for the fatigue evaluation of the system. Likewise, Bayat et al (35) studied the impact of drained and undrained behavior of soil on stiffness and damping of soil-pile interaction of OWT monopile foundations. To this end, a simple Kelvin model was used in a two-dimensional finite element program to simulate a segment of a monopile at different depths subjected to small-magnitude cyclic loading. The authors of that study presented effective stiffness and equivalent damping diagrams of the soil, which can be applied to p-y-$\dot{y}$ models of the Kelvin type.

In the present work, the soil-pile interaction of a monopile-supported OWT is investigated by using four different generalized models (GM) within the Winkler approach, (15). The novelty of the present work lies in the extension of recently-developed mechanical formulations for the shear behavior of high-damping rubber seismic isolators, (36, 37), to describe the nonlinear hysteretic soil behavior. Apart from the fact that the shear strain amplitudes for soil are much smaller compared to rubber, the main difference in the cyclic shear response of soil and high-damping rubber materials, is that the typical equivalent damping versus strain amplitude in the case of soils show an increasing trend with increasing strain amplitude, while in the case of high-damping rubbers the equivalent damping shows a decreasing trend, see e.g. (38, 39). The mechanical models are calibrated against p-y curves provided by the American Petroleum Institute (API) (40). Although the p-y methodology has been proposed many years back (41, 42), and its limitations have been reported in the literature regarding OWT, (4, 44, 45), it is still a common tool used in the industry (34). Furthermore, it should be highlighted that the aim of the current study is to show the ability of the mechanical models presented herein to be calibrated against any kind of soil-pile response curves and that they are able to provide a wide range of hysteretic energy dissipation level under the same effective stiffness.

The mechanical formulations used in the present study are analyzed and explained, and consequently the equation of motion of the overall system is presented. Subsequently, a numerical implementation of the OWT system is performed and to this end the 5MW reference wind turbine of the National Renewable Energy Laboratory (NREL) is used, (46). Moreover, a set of static and dynamic analyses are presented to highlight the key parameters.

2 Mechanical models for soil-pile interaction

The nonlinear pile-soil interaction is often treated by the concept of p-y curves, (40). These monotonic loading curves are extended to cyclic loading by two extreme approaches in the industry. In the first approach, referred to as model 1 in the current study, the kinematic hardening captured by the Iwan model (28) is used. The disadvantage of this model is that it generates large hysteretic damping (as high as 60%) at large displacements, which is unrealistic. More specifically, as it is pointed out by Vucetic and Dobry (39), damping ratio in soil does not exceed $25\% - 30\%$. In the second approach, referred to as model 2 in the current study, the unloading is captured by using the nonlinear elastic concept in which the unloading occurs along the same loading curve. Furthermore, this model generates no damping, which is obviously incorrect. To this end, alternative models are introduced in the present work, which are able to control the damping ratio within acceptable limits for the case of soil, referred to as models 3 and 4. In the rest of the section, the different mechanical components used to compose the four models are introduced, while the assemblage of the elements that constitute the four models used herein (i.e. models 1,2,3,4), is presented in Section 4.

The material properties can be roughly categorized as follows: (i) elasticity, (ii) plasticity and (iii) viscosity, see (47). In the current study, two types of mechanical models are used, namely a trilinear hysteretic model (THM), see Fig. 1 and a hysteretic damper (HD), see Fig. 2. More precisely, in Fig. 1(a) the mechanical formulation of the THM is shown, which consists of a linear spring (element 1) connected in series with a parallel system, namely a plastic slider (element 2) and a trilinear elastic spring (element 3). The plots in Fig. 1 show the force-displacement relationship of the different individual elements of the system, along with the total response (Fig. 1(e)). The mechanical parameters of the THM are the elastic stiffness k_e of element 1, the yield force f_s of element 2, the stiffnesses k_{h1} and k_{h2} and the characteristic displacement u_c of element 3, see Fig. 1(a)(b)(c)(d). The mathematical parameters of the THM are the elastic stiffness k_0, the first postyield stiffness k_1, the second postyield stiffness k_2, the first yield displacement u_y and the second yield displacement u_{yh}, see Fig. 1(e). It should be noted that the mechanical parameters define the properties of the physical model, see Fig. 1(a), while the mathematical ones define the properties of its corresponding force-displacement graph shown in Fig. 1(e). Two sets of parameters are needed because there is no one to one relationship between the parameters of the physical model and its corresponding force-displacement representation, apart from k_e and k_0. The relationships between the mechanical and the mathematical parameters of the THM are presented in Table 1. The compatibility equations along with the equilibrium and constitutive equations of the THM are presented in Table 2. It should be noted that the elastoplastic element (EP) and the trilinear elastic model (TEM) are just particular cases of the THM. More specifically, by providing, in terms of mechanical parameters, an

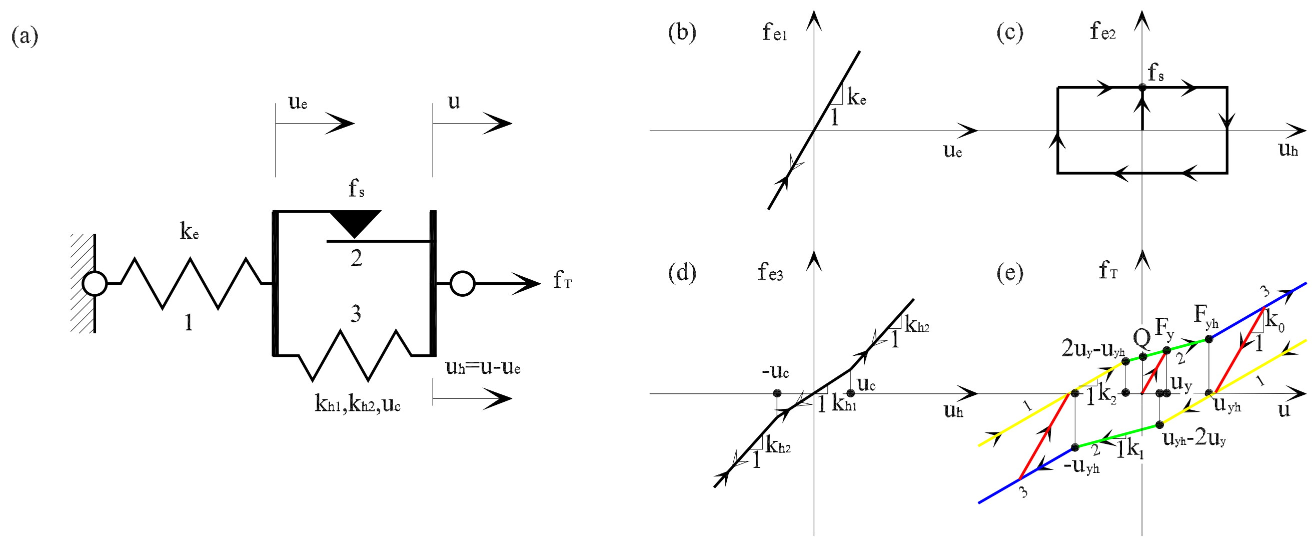

Figure 1: Trilinear hysteretic model (THM): (a) mechanical model, (b) force-displacement loop of the spring element 1, (c) force-displacement loop of the plastic slider element 2, (d) force-displacement loop of the nonlinear spring element 3 and (e) force-displacement loop of the overall model.

elastic stiffness k_e much greater than both stiffnesses k_{h1}, k_{h2} ($k_e >> k_{h1}, k_{h2}$) and by choosing the yield force f_s to be equal to zero ($f_s = 0$) the THM transforms to a TEM (in terms of mathematical parameters would be $u_y = 0$, $k_0 >> k_1, k_2$). On the other hand, by providing the stiffnesses k_{h1}, k_{h2} equal to zero ($k_{h1} = k_{h2} = 0$) the THM is transformed to an EP (in terms of mathematical parameters would be $k_1 = k_2 = 0$).

Additionally, the parameters needed to describe the behavior of the HD are: the elastic stiffness k_{he}, the unloading stiffness k_{hu} and the characteristic displacement u_{hc}, whereas the constitutive equations of the HD are presented in Table 3. The HD is used in order to force the generalized mechanical models to follow a particular unloading stiffness. These type of models have been used in the simulation of the nonlinear behavior of base isolators, see (36).

Lastly, an advanced model comprising a THM connected in parallel with a TEM will be also used for the nonlinear simulation of the soil behavior, see Fig. 3. The THM has the ability to increase the damping while hardening ($k_2 > k_1$) and decrease the damping while softening ($k_2 < k_1$), see (37). The combination of THM with TEM allows for control over the amount of dissipated damping over a cycle, and at the same time provides an unaffected loading path, meaning that the effective stiffness is kept constant, see Fig. 3. For further details on the mechanical models presented herein, the reader is referred to (36, 37).

Table 1: Relationships between mechanical and mathematical parameters of the THM, see Fig. 1(a),(e).

$k_e = k_0$	$k_{h1} = k_1 \frac{k_0}{k_0 - k_1}$	$k_{h2} = k_2 \frac{k_0}{k_0 - k_2}$	$f_s = k_0 u_y = F_y$	$u_c = (u_{yh} - u_y) \frac{k_0 - k_1}{k_0}$

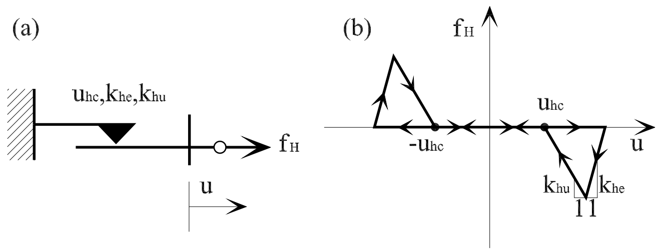

Figure 2: Hysteretic damper: (a) mechanical model, (b) force-displacement loop of the model.

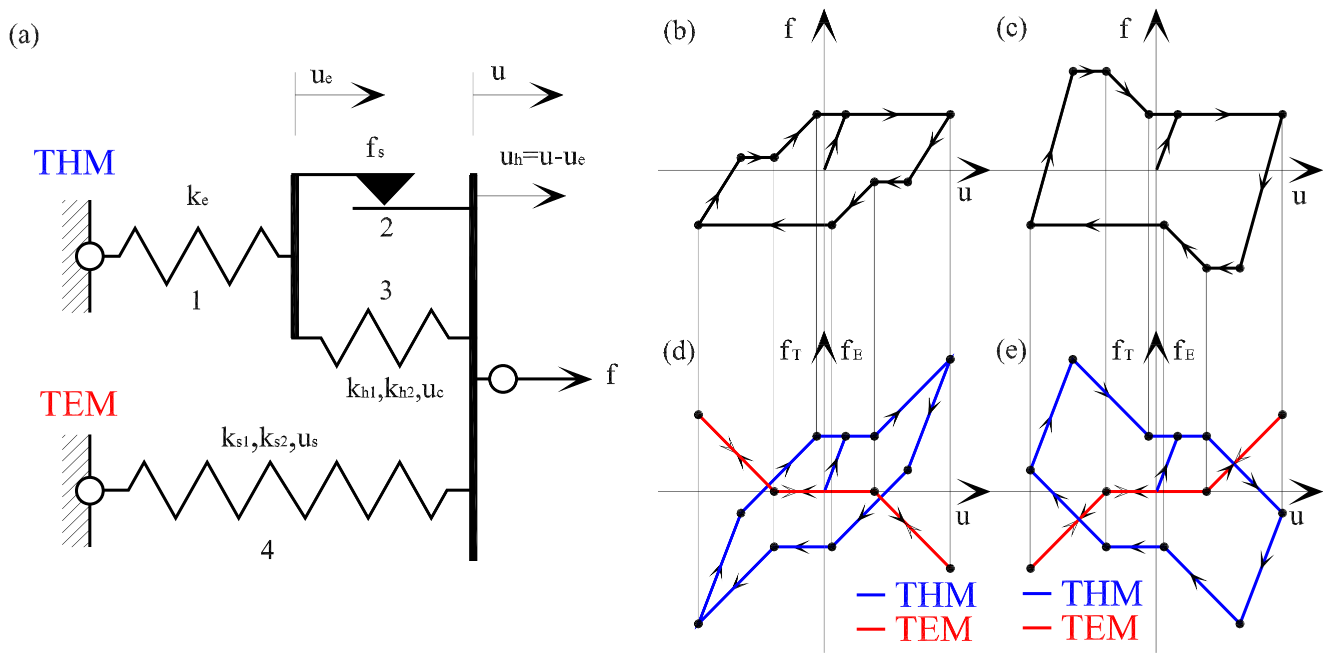

Figure 3: Combination of trilinear hysteretic model (THM) and trilinear elastic model (TEM): (a) mechanical model, (b) force-displacement loop for the hardening case, (c) force-displacement loop for the softening case, (d) force-displacement loop of THM and TEM for the hardening case and (e) force-displacement loop of THM and TEM for the softening case.

3 Equation of motion

The soil-pile-turbine model used in the present study is the 5-MW reference wind turbine developed by NREL, (46). This wind turbine was developed by using publicly available information on different aspects of wind turbines (structural, operational etc) that existed at the time and has been serving as a baseline in research on megawatt-scaled wind turbines. Herein, an equivalent beam/mass model is used to provide the natural frequency of the reference wind turbine. The tower diameter and wall thickness are 6 m and 27 mm at the base respectively. The reader is referred to Jonkman et al, (46) for the description of all the parameters of the reference turbine. The soil in this reference case is sand with the parameters indicated in Fig. 4. A multi-degree-of-freedom (MDOF) system is used to

Table 2: Compatibility, equilibrium and constitutive equations of the THM, see Fig. 1.

compatibility	u	$u_e + u_h$
equilibrium	f_T	$f_{e1} = f_{e2} + f_{e3}$
constitutive	f_{e1}	$k_e u_e$
	$f_{e2}(\dot{u}_h \neq 0)$	$f_s sgn(\dot{u}_h)$
	$f_{e2}(\dot{u}_h = 0)$	$f_{e1} - f_{e3}$
	$f_{e3}(\lvert u_h\rvert \leq u_c)$	$k_{h1} u_h$
	$f_{e3}(\lvert u_h\rvert > u_c)$	$(k_{h1}u_c + k_{h2}(\lvert u_h\rvert - u_c)\, sgn^*(u_h))$

sgn is the signum function

Table 3: Constitutive equations of the HD, see Fig. 1.

$f_H\,(\lvert u\rvert \leq u_{hc})$	0
$f_H\,(\lvert u\rvert > u_{hc}; u\dot{u} \geq 0)$	0
$f_H\,(\lvert u\rvert > u_{hc}; u\dot{u} < 0; elastic)$	$F_{es} + k_{he}\,(u - u_{es})$
$f_H\,(\lvert u\rvert > u_{hc}; u\dot{u} < 0; plastic)$	$k_{hu}\,(u - u_{hc} sgn(u))$

F_{es}, u_{es} are the force and the displacement at the beginning of the elastic phase

k_{hu} is negative

sgn is the signum function

simulate the overall system, see Fig. 4, and its equation of motion can be formulated as follows:

$$\mathbf{M}\ddot{\mathbf{U}}(t) + \mathbf{F}(t) = \mathbf{P}(t) \tag{1}$$

where the resisting force vector is given by

$$\mathbf{F}(t) = \mathbf{K}\mathbf{U}(t) + \mathbf{F}_N(t) \tag{2}$$

In the above equations, $\mathbf{M}$ is the mass matrix, $\ddot{\mathbf{U}}(t)$ is the acceleration array, $\mathbf{F}(t)$ is the restoring force array, $\mathbf{P}(t)$ is the external force array, $\mathbf{K}$ is the stiffness matrix, $\mathbf{U}(t)$ is the displacement array and $\mathbf{F}_N(t)$ is the array of the nonlinear forces.

The mass matrix $\mathbf{M}$ is a diagonal matrix and its main diagonal consists of the lumped masses of the MDOF system, as well as of the moments of inertia of those masses, see Fig. 4. The stiffness matrix $\mathbf{K}$ of the system is a symmetric nine-diagonal matrix, which is assembled by the 4x4 stiffness matrices of the pile elements as well as of

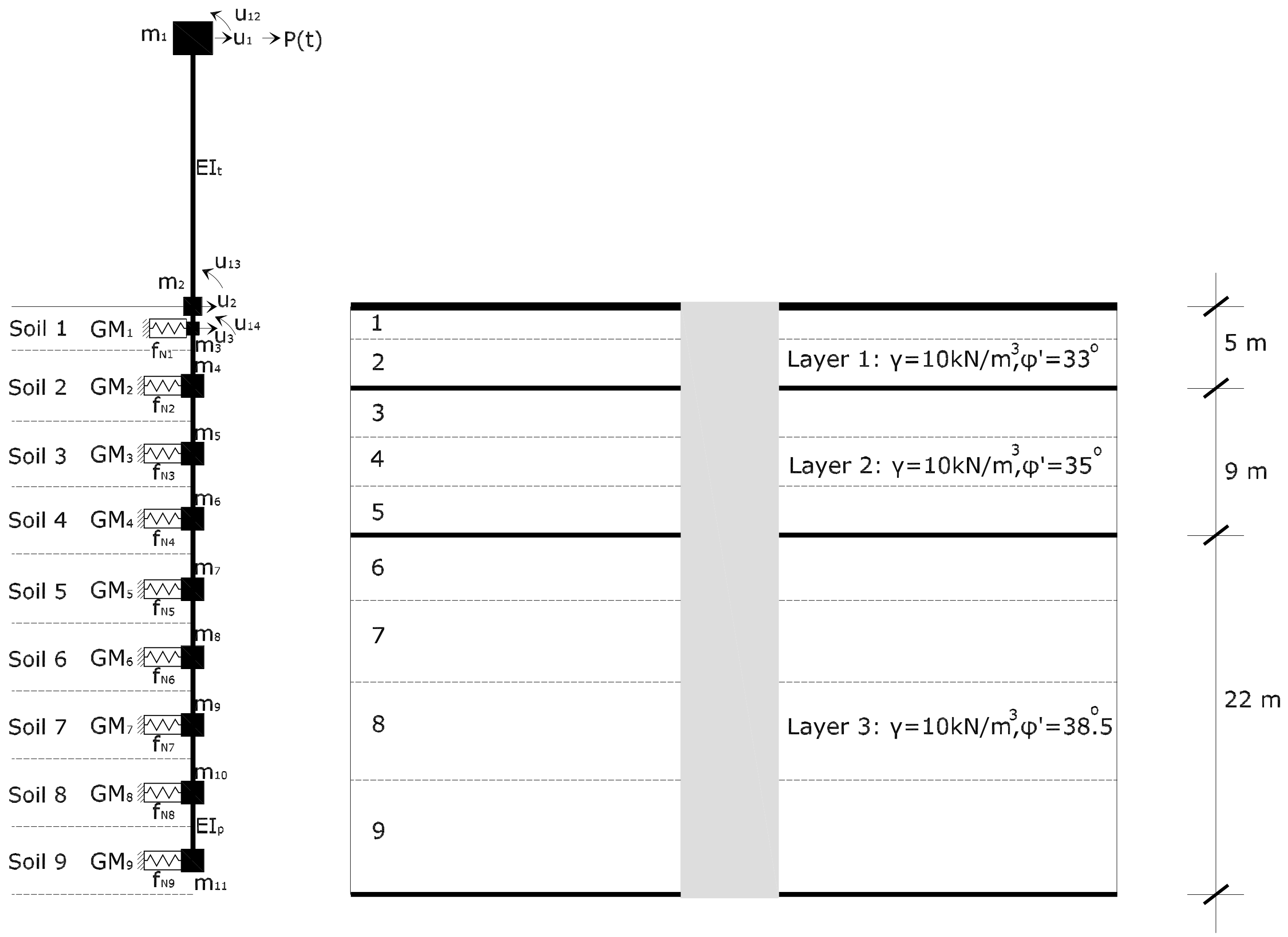

Figure 4: (a) MDOF system of the wind turbine and the monopile foundation and (b) monopile foundation of the 5MW NREL wind turbine.

the superstructure element. Finally, it might be worth noticing that the external force vector $\mathbf{P}(t)$ is applied at the top of the structure.

4 Numerical implementation

In this section the parameters of the systems defined previously are presented. Four different generalized mechanical models are used to describe the behavior of the soil, which are described by the array of the nonlinear forces $\mathbf{F}_N(t)$. In Table 4 the combination of different mechanical elements is presented for each model. Each combination of those elements (ten or fifteen) with different parameters is used to describe each one of the p-y curves presented in Fig. 5. The first model consists of ten EP connected in parallel (model 1), the second one of ten TEM (model 2), the third one consists of five EP and five TEM (model 3), while in the last model the EP of the model 3 were replaced by a combination of a THM with a TEM, see Fig. 3, and five HD were added (model 4). It should be clarified that in the case of model 4, only each of the first four top soil layers are described by model 4, while each one of the remaining ones are described by model 3 with additional five HD.

Model 1 and model 2 are used as extreme cases for comparison and reference purposes in the present study due to the fact that they provide large and zero damping ratio respectively. In order to control the damping ratio and to provide realistic representation of the soil damping, a combination of the two aforementioned models is used and in this way model 3 is obtained. In this case, the damping ratio can be controlled in order to represent the soil behavior within the acceptable limits. The disadvantage of model 3 is that it does not provide unloading stiffness equal to the initial stiffness for large amplitudes and that it does not provide smooth unloading behavior. An alternative way of controlling the damping ratio is to use a more complex model, namely model 4. In this case, the unloading behavior of the model is smoother compared to model 3. Additionally, a series of HD are introduced which ensure that the unloading stiffness of the model is equal to the initial stiffness as it is observed experimentally. The equivalent viscous damping ratio ζ_{eq} is computed as follows:

$$\zeta_{eq} = \frac{1}{4\pi}\frac{E_D}{E_S} \tag{3}$$

where E_D is the dissipated energy in a full hysteresis and E_S is the corresponding strain energy.

Damping has an important role on the fatigue life of OWTs. While during normal operation aeroelastic damping due to blade rotation can be as high as 5%, there is no damping in parked positions. Hence, the damping due to pile-soil interaction, albeit small, has noticeable effect on reduction of the tower vibration.

The parameters of the all models for the top soil layer, see Fig. 5(a), are given in Tables 5- 7 and were calibrated according to API, (40) for sand soil parameters given in Fig. 4. Similar sets of the remaining eight soil layers are used, but they are not presented for brevity. As it is shown in Fig. 4, different parameters (ϕ', γ) are used for different soil layers. The parameter ϕ' denotes the friction angle of the soil, which is used in order to describe the frictional resistance of the soil under shear force, while γ denotes the effective submerged weight of the soil. The soil is split into nine soil layers, see Fig. 4, and the p-y curves of the calibrated models are shown in Fig. 5. It should be noted that the models were calibrated up to maximum displacement equal to 2% of the diameter of the pile, namely $120mm$. All models (model 1, 2, 3 and 4) reproduce the same backbone (loading) curve, but they generate different energy dissipation.

Table 4: Generalized mechanical models for soil-pile interaction.

Elements	**Model 1**	**Model 2**	**Model 3**	**Model 4**
1-5	EP	TEM	EP	THM-TEM
6-10	EP	TEM	TEM	TEM
11-15	-	-	-	HD
Note	EP 	TEM 	THM-TEM 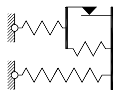	HD 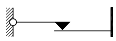

Table 5: Parameters of the elastoplastic elements of the generalized model GM1 used to describe the soil behavior of model 1 and parameters of trilinear elastic elements of the GM1 (see Fig. 4) used for the behavior of the top soil layer of models 1 and 2, see Fig. 5(a).

	Model 1		Model 2		
	Elastoplastic elements		Trilinear elastic models		
Layer	k_0 $\left(\frac{kN}{m}\right)$	Q (kN)	k_{s1} $\left(\frac{kN}{m}\right)$	k_{s2} $\left(\frac{kN}{m}\right)$	u_s (m)
GM1	3449.652	12.074	3449.652	0	0.0035
	3449.652	17.593	3449.652	0	0.0051
	3449.652	22.423	3449.652	0	0.0065
	3449.652	27.252	3449.652	0	0.0079
	3449.652	32.082	3449.652	0	0.0093
	3449.652	37.601	3449.652	0	0.0109
	3449.652	43.811	3449.652	0	0.0127
	3449.652	52.090	3449.652	0	0.0151
	3449.652	64.508	3449.652	0	0.0187
	2331.766	66.455	2331.766	0	0.0285

Table 6: Parameters of the elastoplastic and trilinear elastic elements of the generalized model GM1 (see Fig. 4) used to describe the behavior of the top soil layer of model 3, see Fig. 5(a).

	Model 3				
	Elastoplastic elements		Trilinear elastic models		
Layer	k_0 $\left(\frac{kN}{m}\right)$	Q (kN)	k_{s1} $\left(\frac{kN}{m}\right)$	k_{s2} $\left(\frac{kN}{m}\right)$	u_s (m)
GM1	3449.652	12.074	3449.652	0	0.0051
	3449.652	22.423	3449.652	0	0.0079
	3449.652	32.082	3449.652	0	0.0109
	3449.652	43.811	3449.652	0	0.0151
	3449.652	64.508	2331.766	0	0.0285

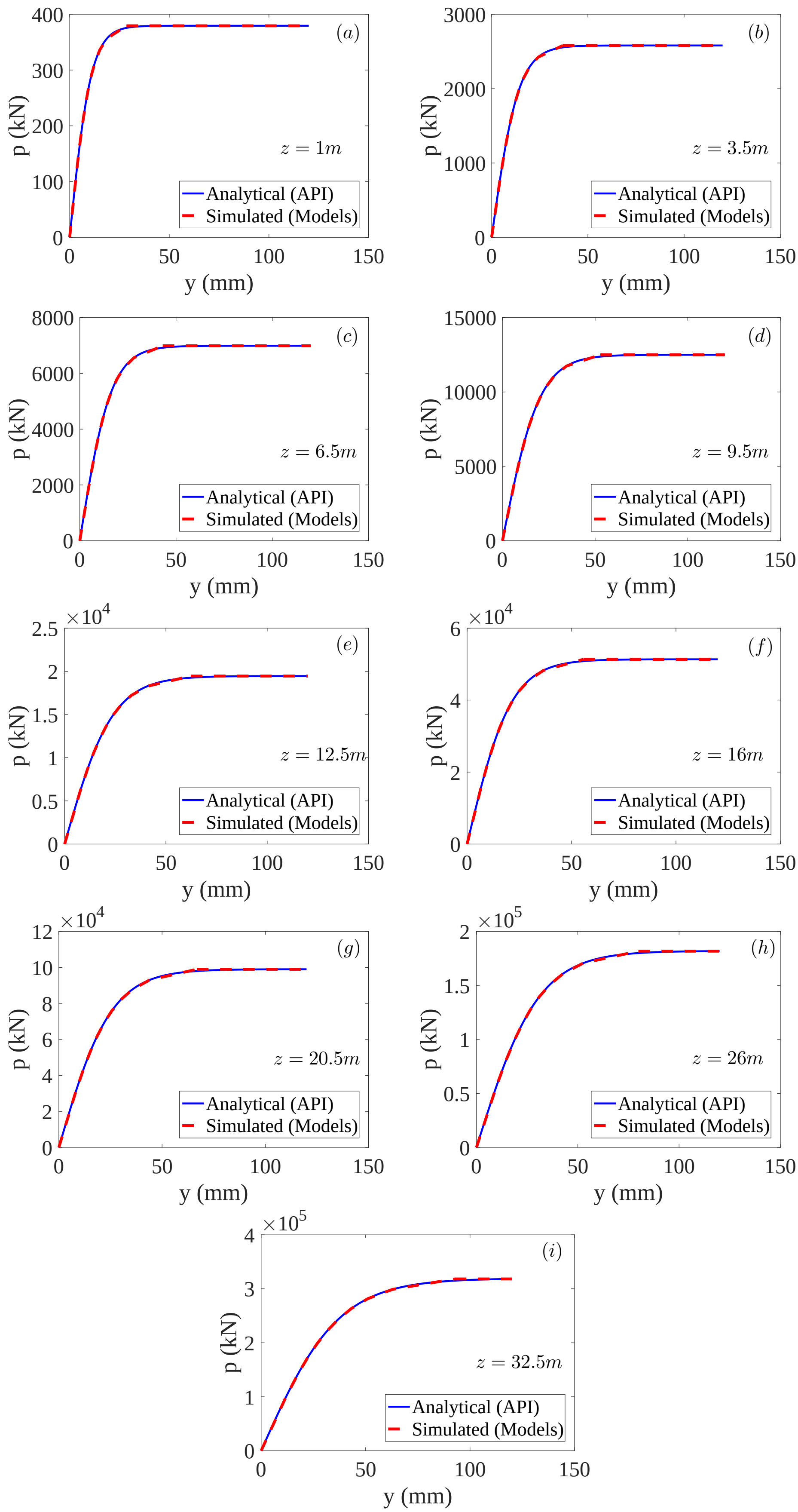

Figure 5: Calibration of the loading curves produced by the models (1, 2, 3, 4) against analytical p-y curves by API for all soil layers.

Table 7: Parameters of the trilinear hysteretic and trilinear elastic elements of the generalized model GM1 (see Fig. 4) used to describe the behavior of the top soil layer of model 4, see Fig. 5(a).

Model 4											
	Trilinear hysteretic models					Trilinear elastic models			Hysteretic dampers		
Layer	k_0 $\left(\frac{kN}{m}\right)$	k_1 $\left(\frac{kN}{m}\right)$	k_2 $\left(\frac{kN}{m}\right)$	u_y (m)	u_{yh} (m)	k_{s1} $\left(\frac{kN}{m}\right)$	k_{s2} $\left(\frac{kN}{m}\right)$	u_s (m)	k_{he} $\left(\frac{kN}{m}\right)$	k_{hu} $\left(\frac{kN}{m}\right)$	u_{hc} (m)
GM1	3449.652	0	379.354	0.0035	0.02	0	-379.354	0.02	3449.652	-100	0.0051
	3449.652	0	758.709	0.0065	0.03	0	-758.709	0.03	3449.652	-100	0.0079
	3449.652	0	1138.063	0.0093	0.05	0	-1138.063	0.05	3449.652	-100	0.0109
	3449.652	0	1517.417	0.0127	0.08	0	-1517.417	0.08	3449.652	-100	0.0151
	3449.652	0	1896.772	0.0187	0.11	0	-1896.772	0.11	2331.766	-100	0.0285
						3449.652	0	0.0051			
						3449.652	0	0.0079			
						3449.652	0	0.0109			
						3449.652	0	0.0151			
						2331.766	0	0.0285			

5 Analyses

The results of the analyses are grouped in two parts: the static and the dynamic one. The constant average acceleration Newmark's method, is used for the analyses, (48).

5.1 Static analysis

The static loading case implies the application of a slow sinusoidal (cyclic) force on top of the pile while the superstructure is not considered. As examples, the force-displacement loops for the top and third soil layers are shown in Fig. 6 for the different models. The results clearly indicate how the hysteretic areas of the loops can be controlled by models 3 and 4. More specifically, models 3 and 4 are able to reduce the dissipated energy, hence damping, more than one half compared with model 1 in the case of the top soil layer. Additionally, in the same figures it is shown that model 4 provides a smoother transition during unloading phases compared with model 4. Furthermore, the results show that only models 1 and 4 provide an unloading stiffness equal to the initial stiffness. It is also worth pointing out that the nonlinear elastic model 2 does not provide any energy dissipation, because it loads and unloads on the same path. Finally, it should also be noticed that as expected, the displacement amplitude in the top soil layer is larger (Fig. 6(a)) compared with the third soil layer shown in Fig. 6(b).

Figure 7 represents the response at the top of the monopile in terms of force-displacement loops, while Fig. 8 displays the corresponding equivalent damping ratios and the ratios of the effective stiffness to the maximum stiffness for the different models. First of all, Fig. 8(c),(d) clearly show that all models provide the same stiffness ratio, while Fig. 8(a),(b) indicate that the damping ratio varies significantly. More specifically, model 1 provides the largest damping ratio (Figs. 7(a) and 8(a),(b)), while model 2 zero damping ratio (Figs. 7(b) and 8(a),(b)). Models 3 and 4

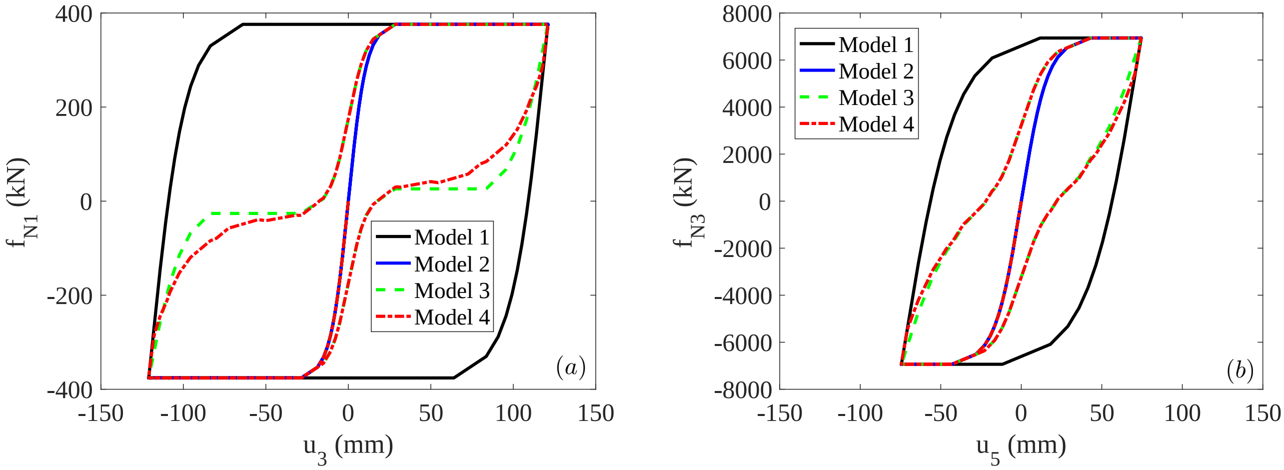

Figure 6: Force-displacement loops on (a) the top and (b) third soil layer for maximum amplitude for statically applied force at the top of the monopile for four models: model 1, model 2, model 3 and model 4.

provide the same amount of damping, that is about half of the damping in model 1 for all displacement amplitudes. The difference between models 3 and 4 can be barely seen in the unloading phases of the force-displacement loops shown in Fig. 7(a). Therefore, it can be concluded that the models provide the same response at the top of the monopile.

Finally, Fig. 9 represents the static response at the top of the monopile for a one-way cyclic loading, which usually is the case for monopile testing. Once again, the results show the differences of the response at the top of the monopile. More precisely, the nonlinear elastic model (model 2) provides a totally unrealistic behavior by loading and unloading on the same path. On the other hand, in Fig. 9(a) the ability of models 3 and 4 to reduce the hysteretic area is clearly shown. The difference between models 3 and 4 can be observed in the unloading phase of the force-displacement loop of Fig. 9(a), whereas models 1 and 4 follow the same unloading stiffness with the initial one, while model 3 provides a reduced unloading stiffness compared with the initial one. Nevertheless, the difference between models 3 and 4 in terms of the response at the top of the monopile is negligible.

5.2 Dynamic analyses

The dynamic analyses are implemented in different groups, which correspond to different types of excitation, namely free vibration and harmonic excitations. In addition, a comparison between responses for different frequency excitations is presented. In all dynamic cases, the superstructure is included and the forces are applied at the top of the superstructure.

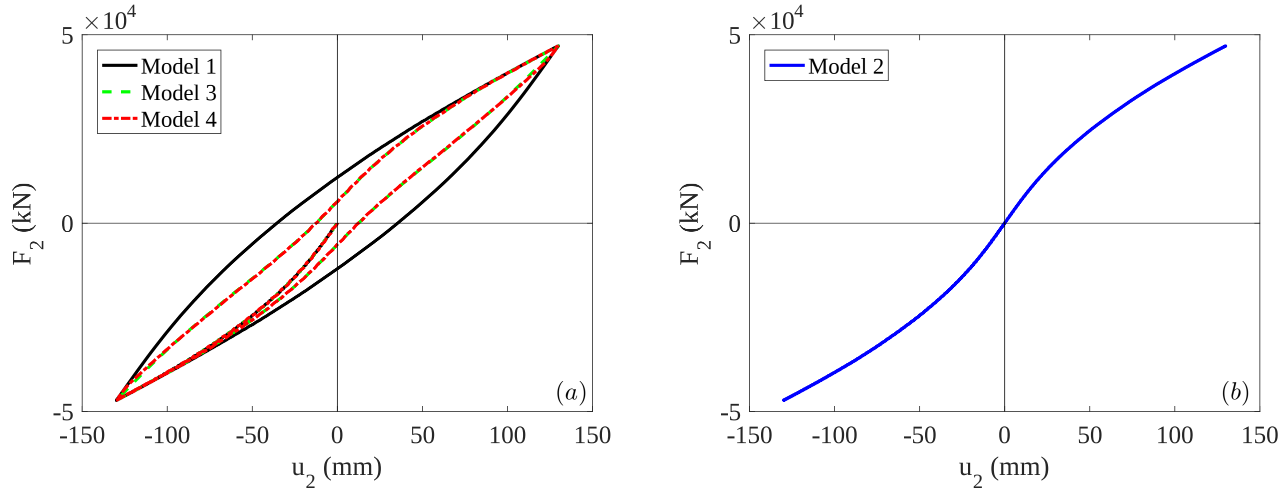

Figure 7: Force-displacement loops on the top of the monopile for statically applied force at the top of the monopile for four models: (1) model 1, model 3, model 4 and (b) model 2.

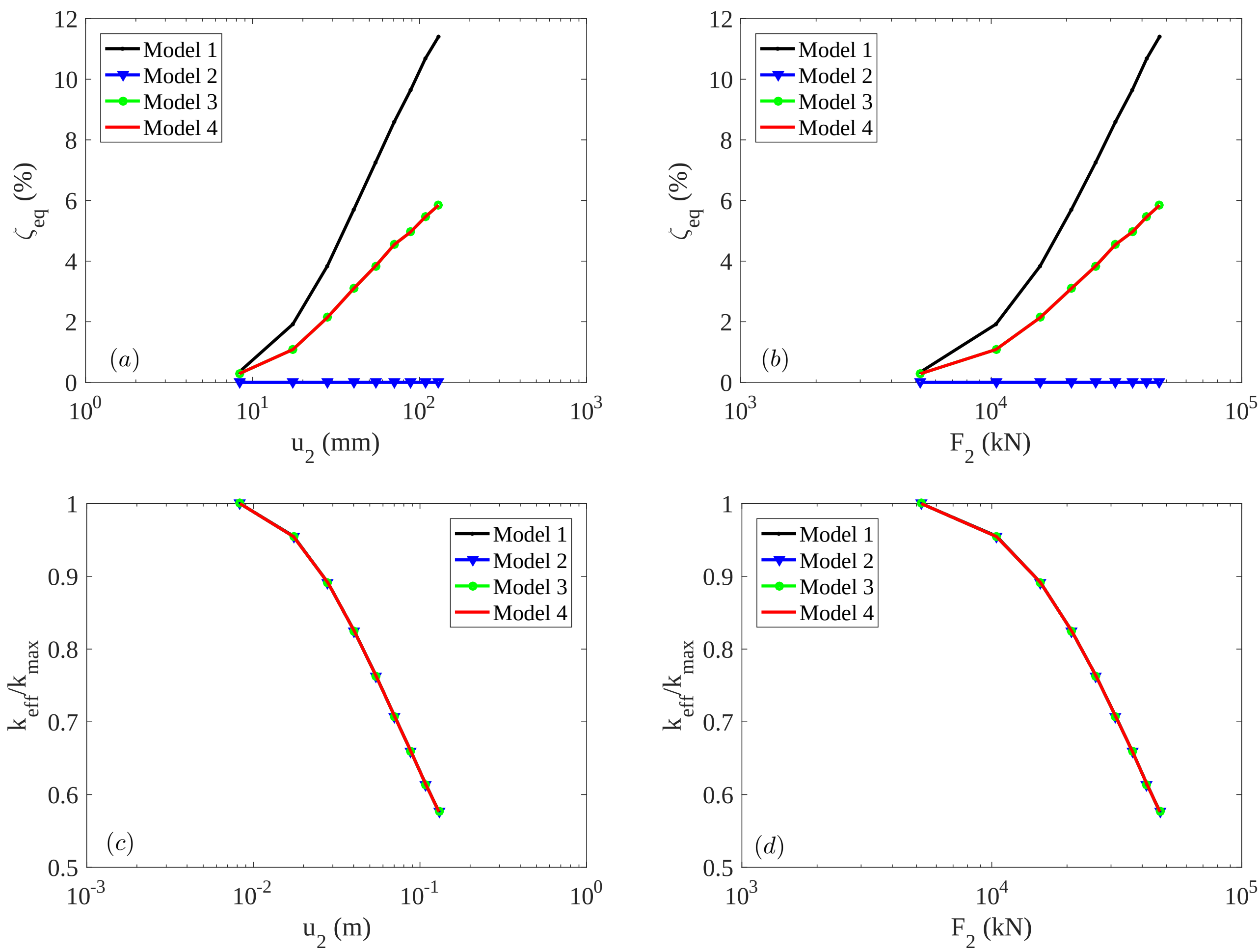

Figure 8: Equivalent viscous damping vs: (a) maximum displacement, (b) maximum force and effective stiffness ratio vs: (c) maximum displacement, (d) maximum force, on the top of the monopile for statically applied force at top of the monopile for four models.

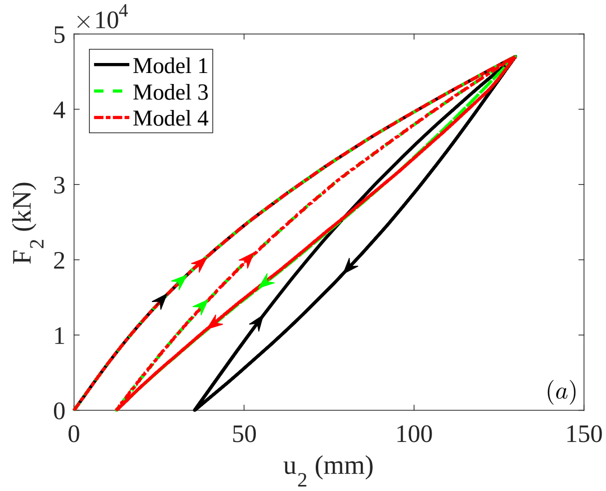

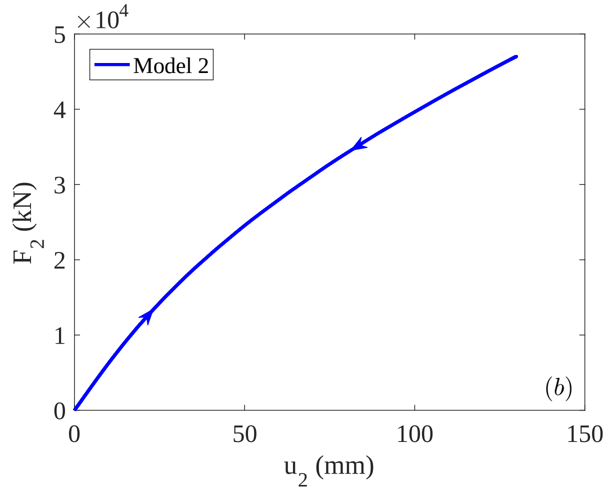

Figure 9: Force-displacement loops on the top of the monopile for statically applied force in one direction at the top of the monopile for four models: (a) model 1, model 3, model 4 and (b) model 2.

5.2.1 Free vibration

In this section free vibration responses of the models are studied by applying initial displacement at the top of the OWT. The results of the free vibration response are presented in Fig. 10 in terms of displacement and rotation histories, while Fig. 11 shows the force-displacement loops of the top soil layer for different models. Again, it should highlighted that the response of model 2 is unrealistic, due to the fact that the response in terms of displacement and rotation amplitudes does not show any decay with time (Fig.10). On the other hand, the response provided by model 1 shows a decay in terms of displacement amplitude of almost 36% in the eighth cycle of vibration, while in terms of rotation the decay is almost equal to 34% compared with model 2. Models 3 and 4 provide the same response in terms of displacement and rotation history as it is shown in Fig. 10. More specifically, the reduction of the displacement amplitude in the eighth cycle of vibration is equal to 21%, while in terms of rotation the amplitude of vibration is reduced of about 20% for both models compared with model 2. As it was also observed in the static analysis, model 1 generates large amounts of energy dissipation, model 2 does not provide any damping, while models 3 and 4 are able to control the damping ratio to acceptable limits. It should be noted that model 4 represents a smoother variation compared to model 3.

5.2.2 Harmonic excitation

Real environmental loads (wave and wind) are irregular, and OWTs are analyzed for many combinations of these loads. One could perform such studies with the help of the presented model. However, harmonic loads at selected frequencies are selected for better visualization of the load effects and highlighting the differences in the models. In this section the results for two different harmonic cases, which correspond to excitation frequencies of f_r=0.30Hz and

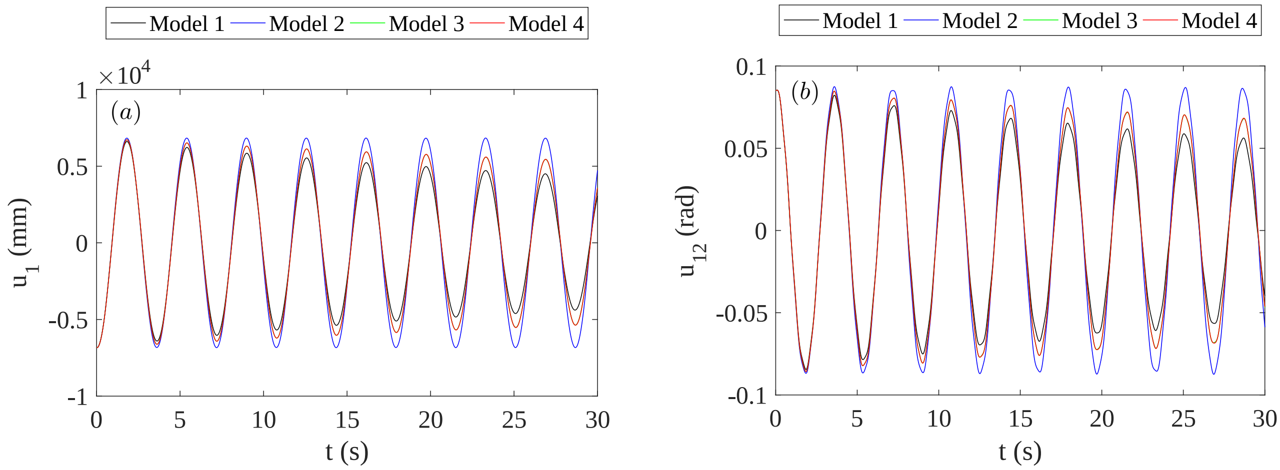

Figure 10: Comparison of (a) displacement histories and (b) rotation histories at the top of the OWT under free vibration excitation at high input displacement.

f_r=0.50Hz are presented. The excitation frequency of 0.30Hz is close to the resonance frequency of the tower, which is 0.32Hz. In Fig 12 the response at the top of the OWT is shown in terms of displacement and rotation history, while in Fig. 13 the force-displacement loops of the models are presented for f_r=0.30Hz. The results in terms of displacement and rotation history do not display large differences. This is because the pile is much stiffer compared with the superstructure and therefore the dynamic response of the system is dominated by the superstructure. This is often the case in real design of OWTs. Nevertheless, the difference in terms of response between unrealistic models 1 and 2 and the more realistic models 3 and 4 cannot be neglected. More specifically, the reduction of the response in terms of displacement amplitude at the eighth cycle of vibration of model 1 relative to model 2 is of the order of 20%, while for models 3 and 4 the reduction is of the order of 10%. Furthermore, in terms of rotation amplitude model 1 provides reduction of around 17% compared with model 2 for the eighth cycle of vibration, while models 3 and 4 provide reduction of around 10%.

In Fig. 14 the results in terms of displacement and rotation histories at the top of the OWT are presented for excitation frequency $f_r = 0.50Hz$. In this case, the maximum reduction of the displacement response between model 1 compared with model 2 is of the order of 35%, while in the case of models 3 and 4 the reduction is of the order of 22%. In terms of rotation response, the maximum reduction between model 1 in comparison with model 2 is of the order of 37% while models 3 and 4 provide a reduction of the order of 25%. Because the excitation frequency of 0.50Hz is outside of the resonance region, it is possible to better observe the differences between the models.

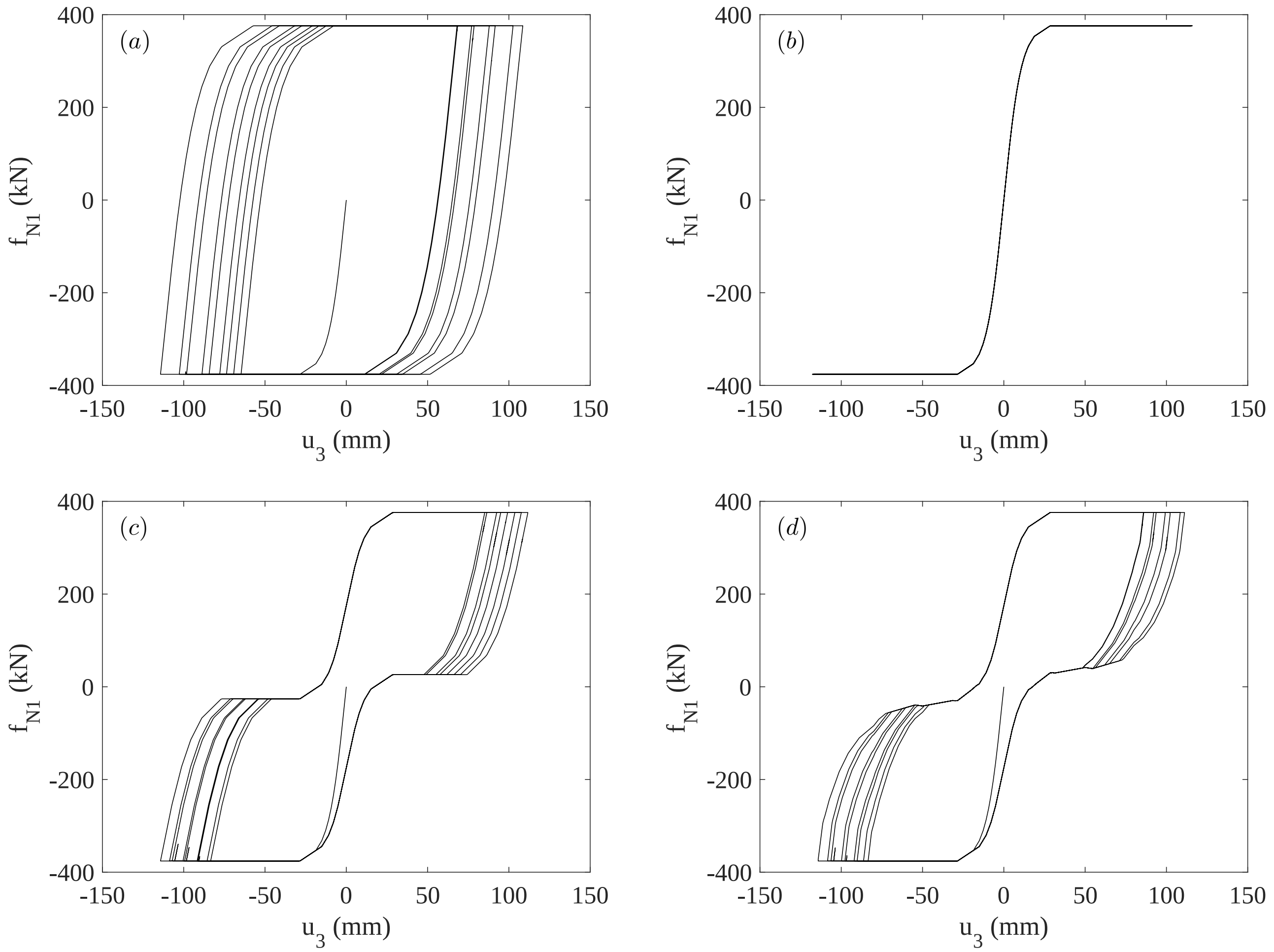

Figure 11: Force displacement loops at the top soil layer under free vibration excitation at high input displacement for (a) model 1, (b) model 2, (c) model 3 and (d) model 4.

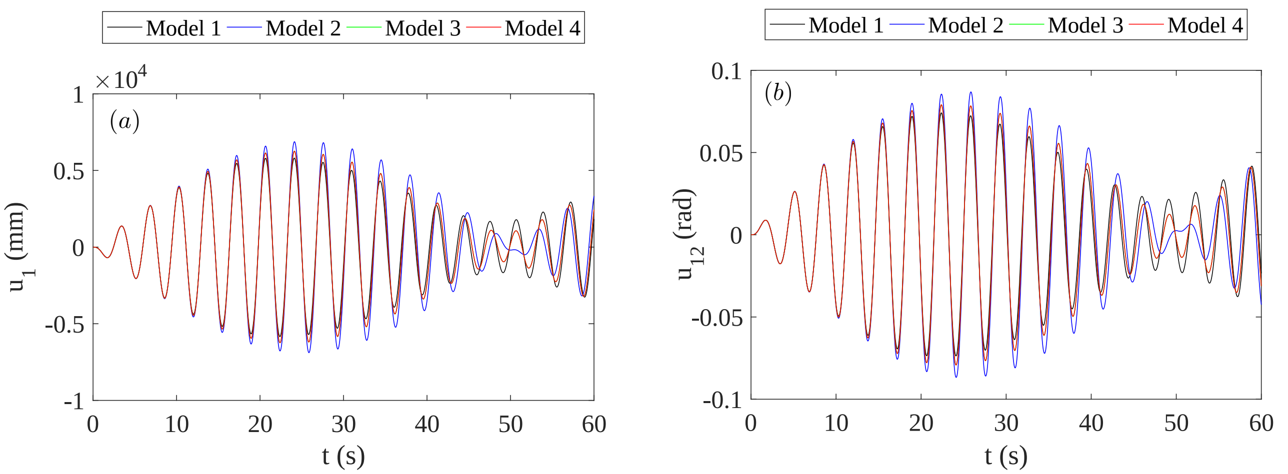

Figure 12: (a) Displacement history and (b) rotation history at the top of the OWT by using model 1, model 2, model 3 and model 4 for frequency $0.30Hz$.

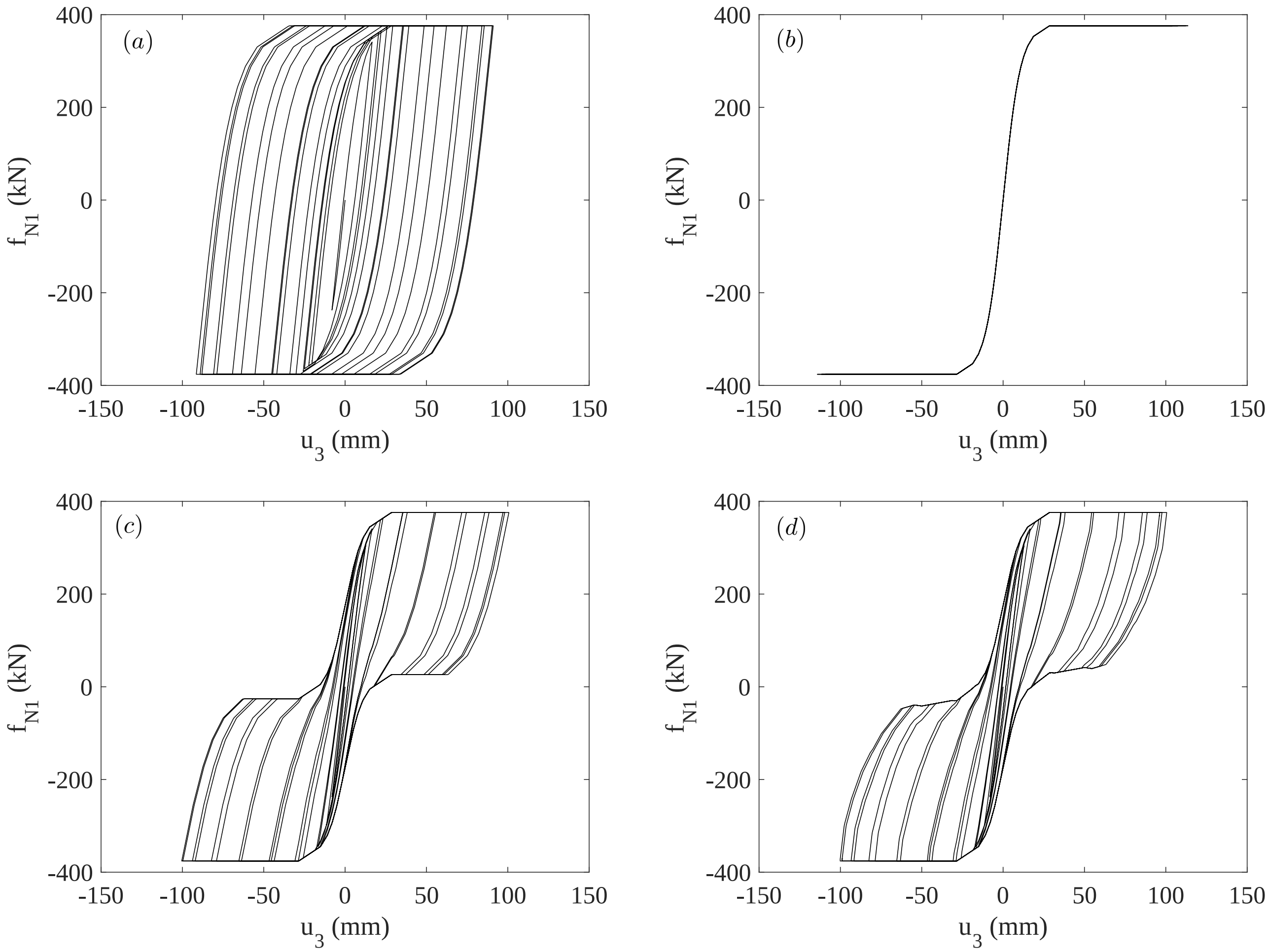

Figure 13: Force-displacement loops of the first soil spring for frequency $0.30Hz$ for (a) model 1, (b) model 2, (c) model 3 and (d) model 4.

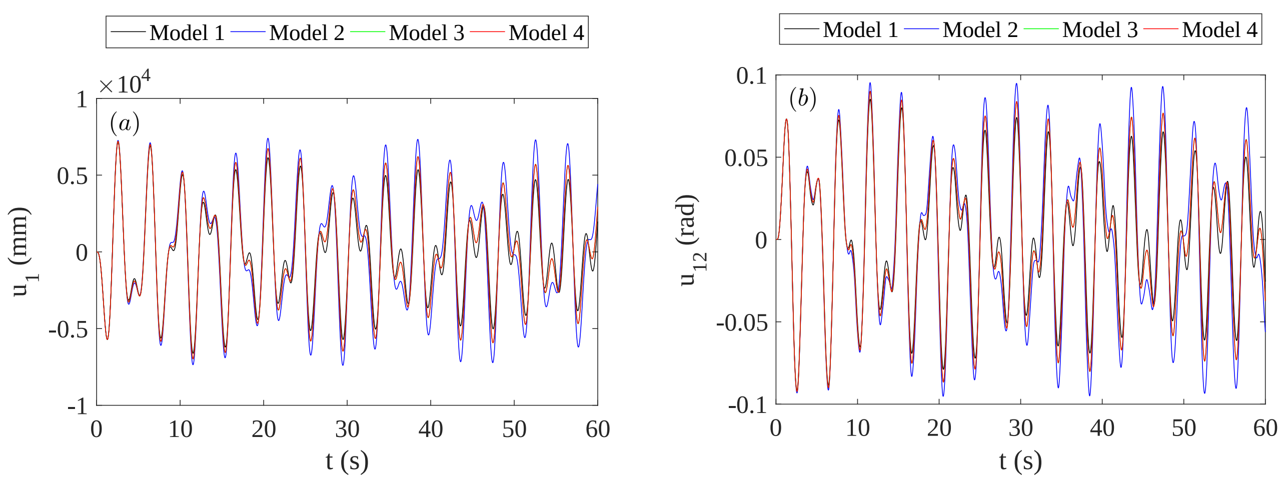

Figure 14: (a) Displacement and (b) rotation history at the top of the OWT by using model 1, model 2, model 3 and model 4 for frequency $0.50Hz$.

5.2.3 Comparison between harmonic excitations

In this section the results of three different harmonic loading cases are compared for the four models. The results are presented in terms of moment-rotation plots at the top of the OWT in Fig. 15 for different models. In this figure, the excessive rotation imposed by the load of 0.30Hz is clearly shown for all models. As it was explained in the previous section, the dynamic response of the system is dominated by the frequency of the tower close to the resonance region, because the foundation is much stiffer than the superstructure. Furthermore, Fig. 15 shows that model 2 predicts larger forces and rotations at the top of the OWT compared with the other three models. Figures 16 and 17 present the results in terms of displacement and rotation histories at the top of the OWT for different models and different excitation frequencies. Once again, the effect of the resonance frequency, namely 0.30Hz, on the response of the system is clearly demonstrated. Excitation frequency of 0.15Hz provides larger excitation response for all models compared with the excitation frequency of 0.50Hz. The fact that all models provide similar response amplitudes in the aforementioned cases can be explained by realizing that for small response amplitudes the models provide similar behavior. Figure 18 shows the response of the top soil layer for different models and excitation frequencies. As it was observed in the previous loading cases, the results show the unrealistic behavior of the nonlinear elastic model, the large amount of energy dissipation provided by model 1, the controlled amount of energy dissipation provided by model 3 and the smoother version of model 3, namely model 4.

Finally, in Fig. 19 the maximum absolute response in terms of displacement and rotation is presented for different models, excitation frequencies and amplitudes. As already described the maximum response for all amplitudes and models is observed for excitation frequency 0.30Hz, while the smallest response is provided by excitation frequency 0.50Hz. The maximum response at the top of the tower is amplified by a factor of 1.1 when the nonlinear elastic model is used instead of models 3 or 4 and by a factor of around 1.2 when the nonlinear elastic model is used instead of model 1 for excitation frequency 0.30Hz. An interesting conclusion from Fig. 19 is that for frequencies outside the resonant region of the tower, the maximum responses are fairly similar for all models. As explained earlier, this is due to the fact that the response is dominated by the tower due to its high flexibility compared to the foundation. While the developed model was used in offshore wind application, there are other examples, such as bridges, that the stiffness contrast between the structure and the foundation is less and the foundation is exposed to larger loads in which cases the damping characteristics of the pile become more decisive in analyzing the response.

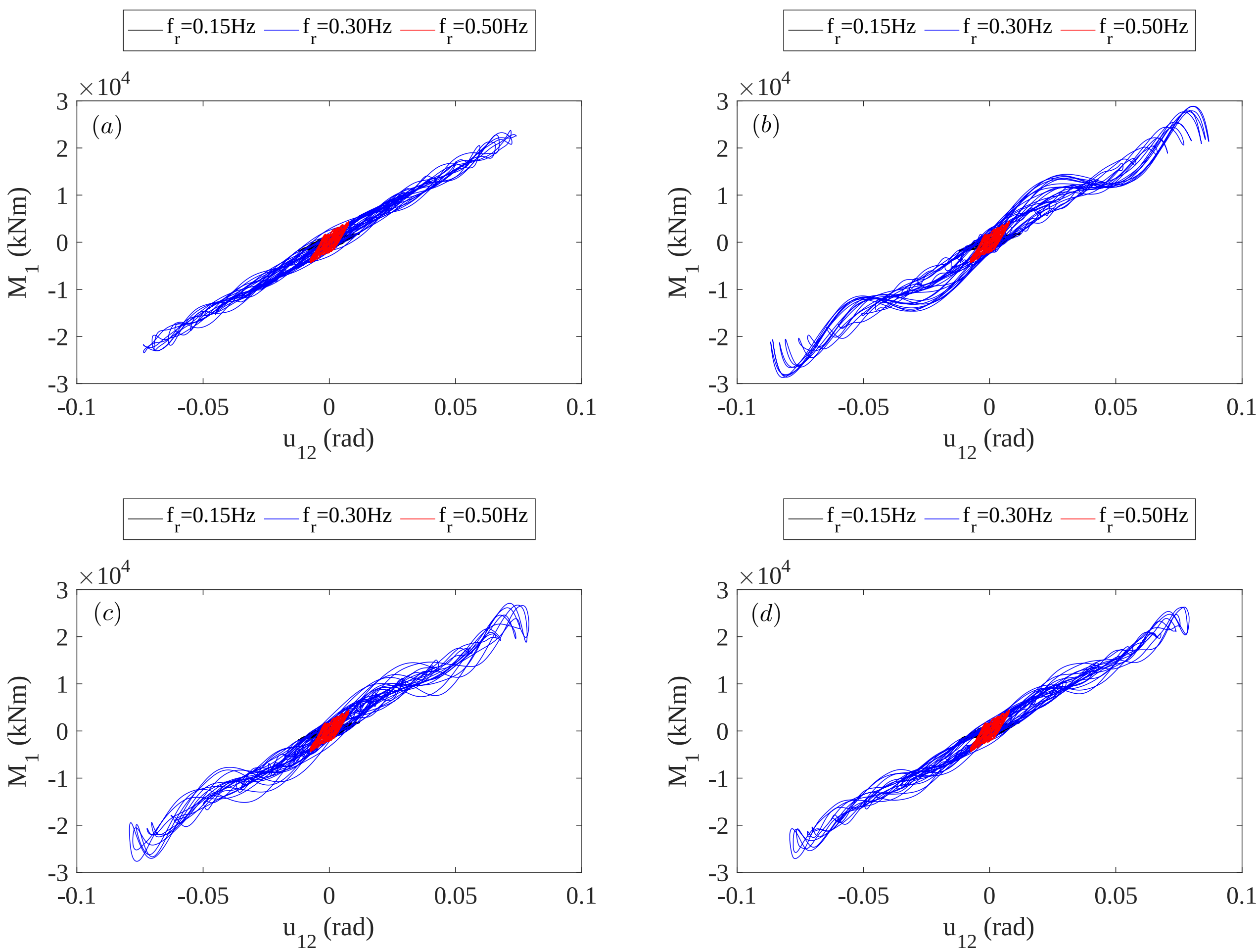

Figure 15: Moment-rotation loop at the top of the OWT by using (a) model 1, (b) model 2, (c) model 3 and (d) model 4 for different excitation frequencies at high excitation amplitude.

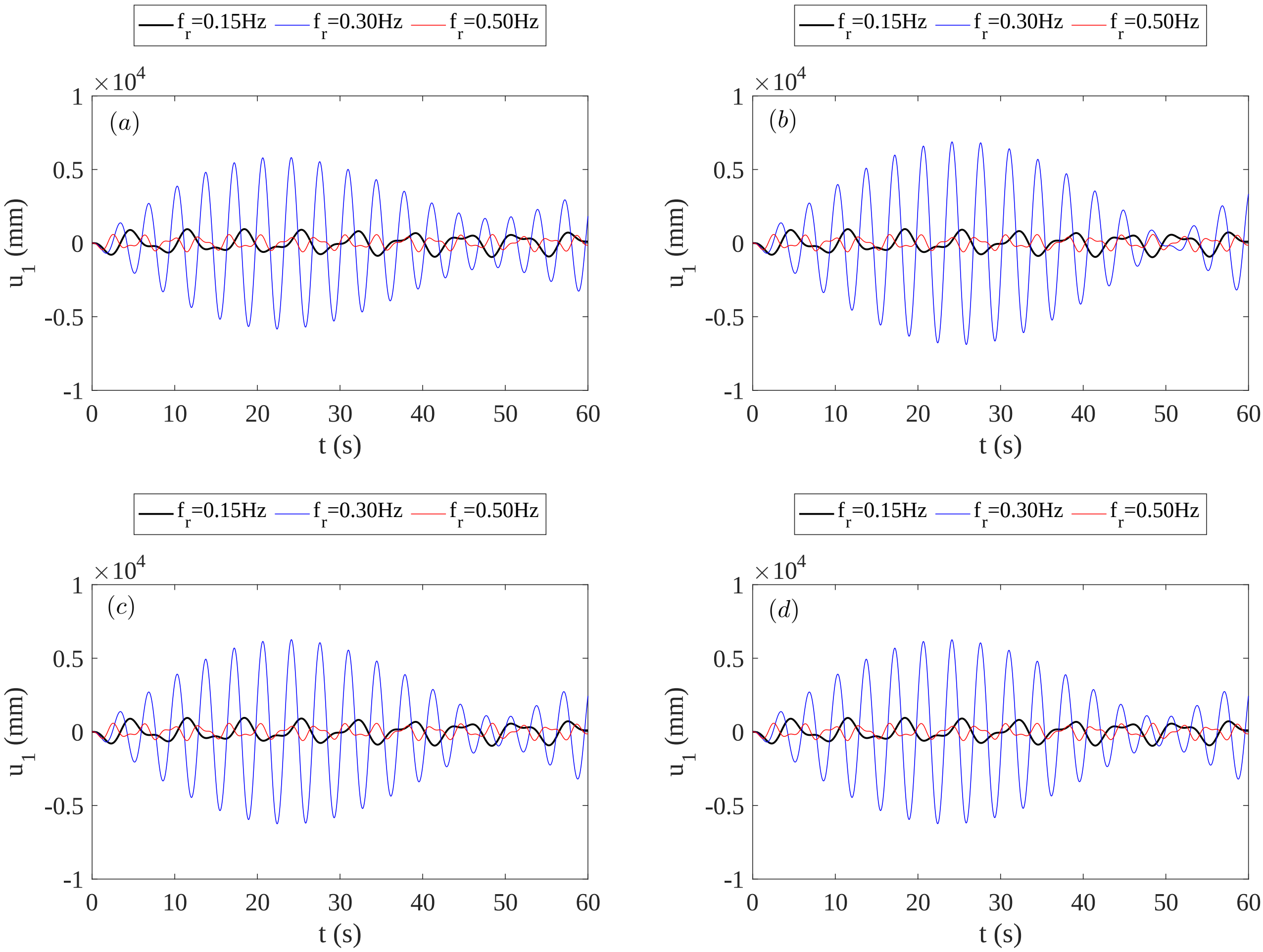

Figure 16: Displacement history at the top of the OWT by using (a) model 1, (b) model 2, (c) model 3 and (d) model 4 for different excitation frequencies at high excitation amplitude.

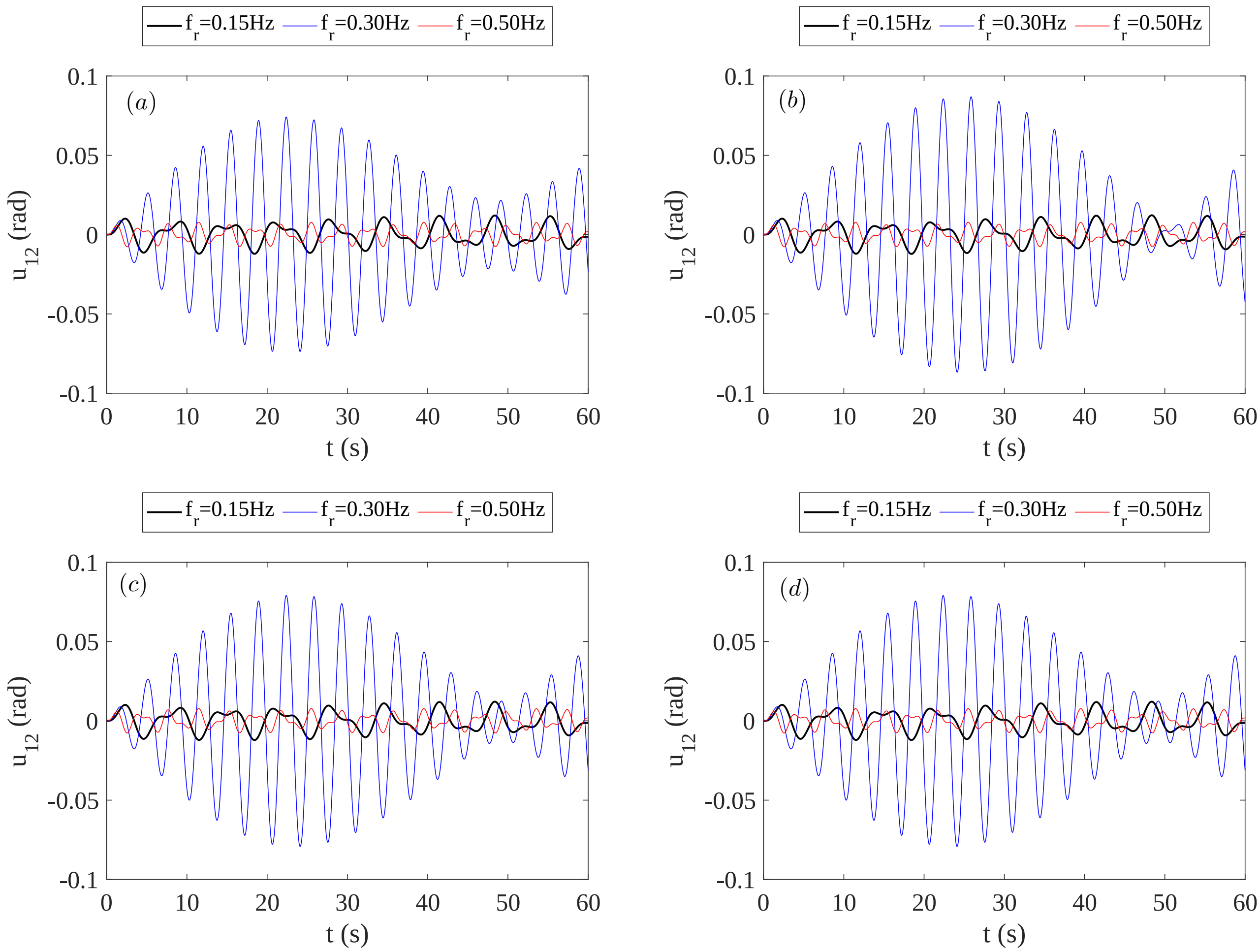

Figure 17: Rotation history at the top of the OWT by using (a) model 1, (b) model 2, (c) model 3 and (d) model 4 for different excitation frequencies at high excitation amplitude.

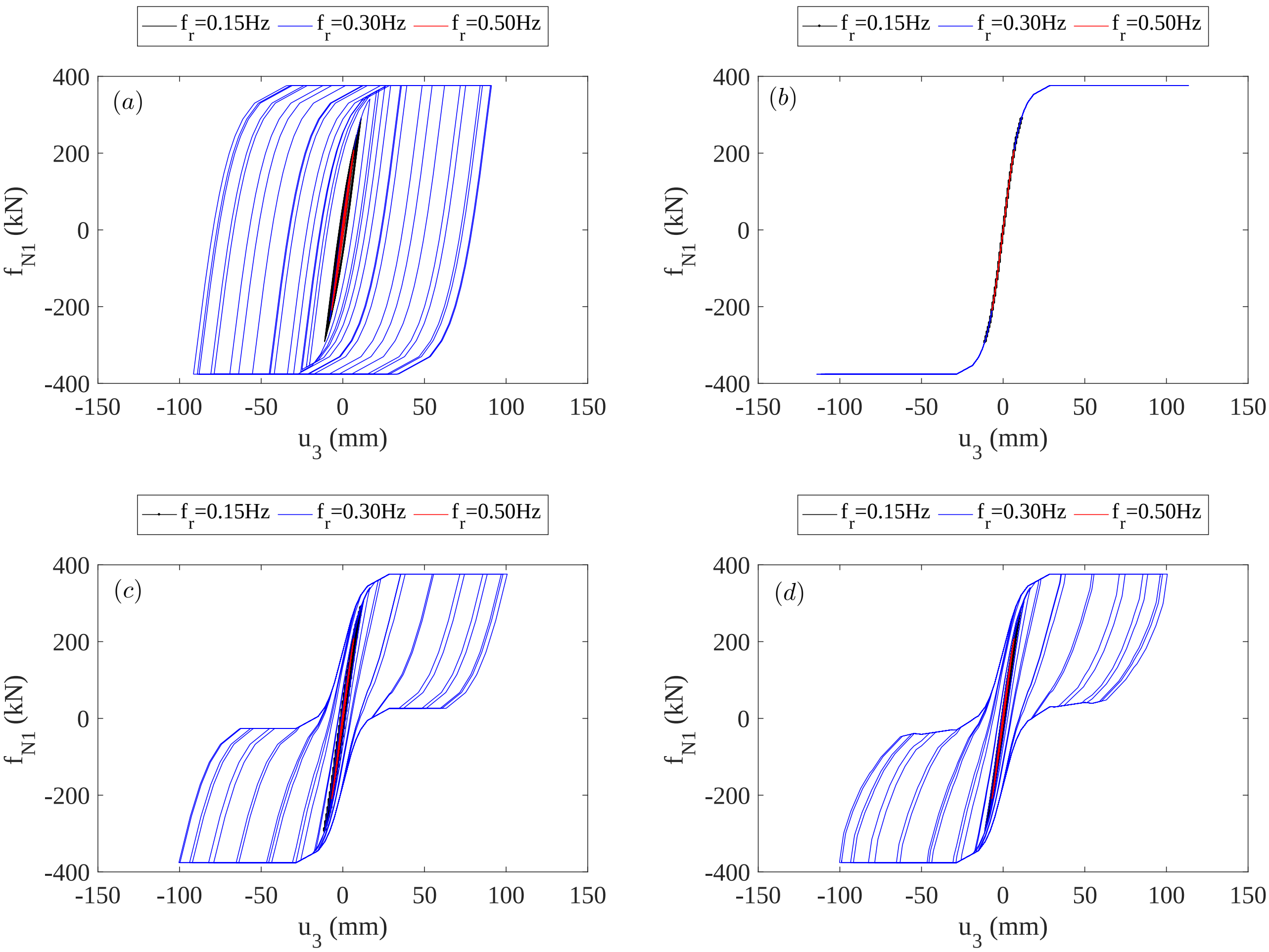

Figure 18: Force-displacement loops of the first soil spring by using (a) model 1, (b) model 2, (c) model 3 and (d) model 4 for different excitation frequencies at high excitation amplitude.

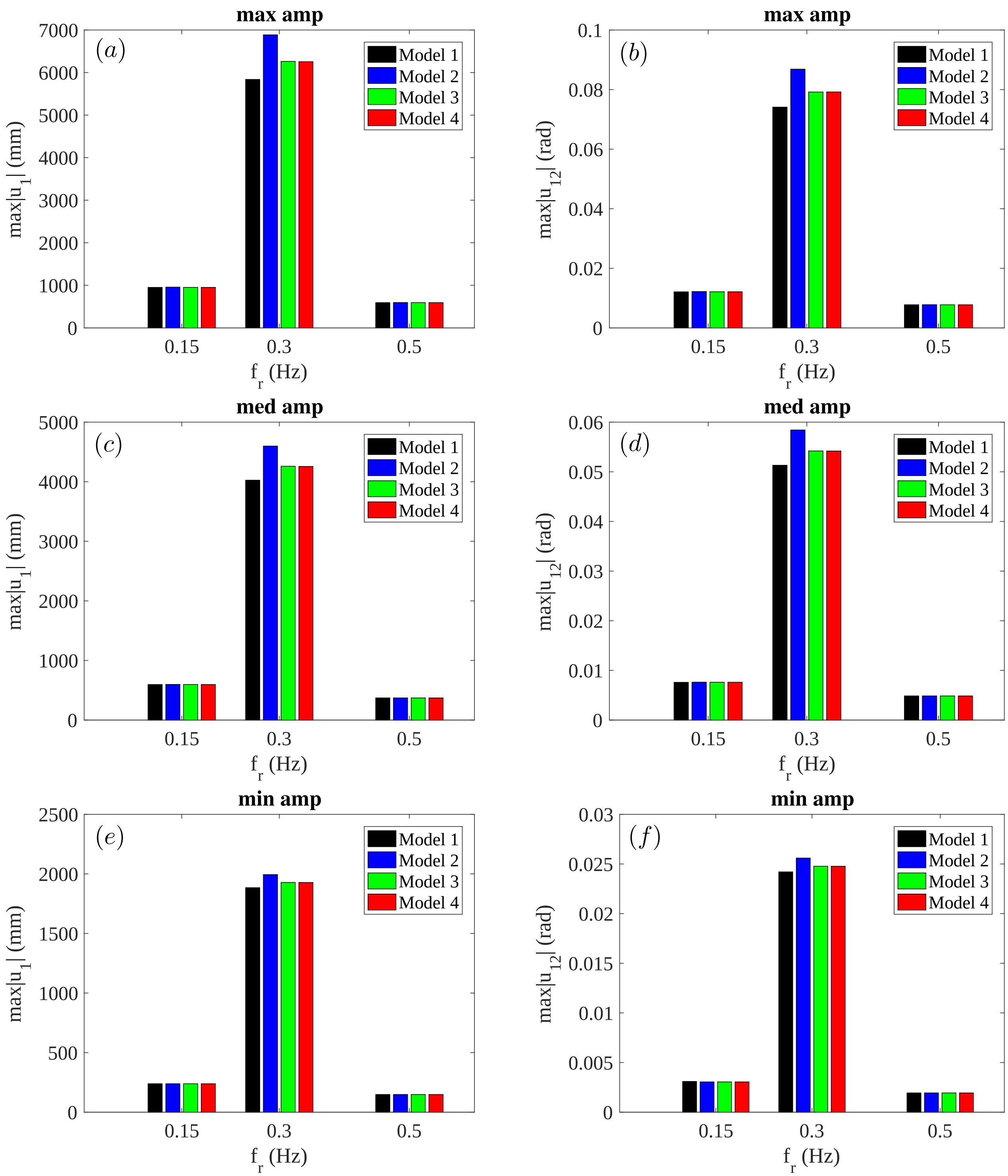

Figure 19: Maximum response at the top of the OWT for different frequencies (a) maximum displacement $max|u_1|$ at high excitation amplitude, (b) maximum rotation $max|u_{12}|$ at high excitation amplitude, (c) maximum displacement $max|u_1|$ at medium excitation amplitude (d) maximum rotation $max|u_{12}|$ at medium excitation amplitude, (e) maximum displacement $max|u_1|$ at low excitation amplitude and (f) maximum rotation $max|u_{12}|$ at low excitation amplitude.

6 Conclusions

The present study is focused on the realistic representation of damping in soil-pile interaction. To this end, recently developed generalized nonlinear mechanical formulations used for the simulation of the behavior of high-damping rubber bearings were introduced successfully to account for nonlinear soil behavior within the soil-pile interaction approach of OWTs. To this end, the mechanical formulations, presented herein as models 3 and 4, are suggested for the simulation of soil-pile interaction within the Winkler type of approach for OWT systems. Both models are able to control the level of damping under constant effective stiffness. Model 4 provides more options in terms of smoother and more realistic transition in the unloading phases. Another advantage of model 4 is that it is able to provide unloading stiffness equal to the initial one. On the other hand, the advantage of model 3 is its simplicity in implementation compared with model 4.

This study highlights that the most commonly models used within the industry practice, namely models 1 and 2, are inappropriate to describe the soil-pile interaction phenomena. More specifically, model 1 underestimates the response of OWTs, due to the excessive amount of damping that it provides, see Fig. 19(a),(b). On the other hand, model 2 overestimates the response of the OWT, due to its unrealistic behavior that provides zero damping ratio, see Fig. 19(a),(b). Subsequently, more appropriate models should be used to account for soil-pile interaction phenomena, such as either simpler model 3 or more advanced model 4, presented in the present study. Finally, the current work emphasizes on the importance that the proper simulation of the soil-pile interaction phenomena has for the estimation of the fatigue lifetime of OWTs, see also (5, 21, 25, 29, 34).

Acknowledgments

This work was supported by the Horizon 2020 MSCA-RISE-2015 project No. 691213 entitled “Experimental Computational Hybrid Assessment of Natural Gas pipelines Exposed to Seismic Risk”. The second author additionally acknowledges partial support from the project "Reducing cost of offshore wind by integrated structural and geotechnical design (REDWIN)" funded by the Norwegian Research Council under Grant 243984. Finally, the authors would also like to thank the anonymous reviewers for their insightful comments and observations.

References

1. Transportation Research Board. *Structural Integrity of Offshore Wind Turbines.* Special Report 305: The National Academies; 2011.

2. Manwell JF, McGowan JG, Rogers AL. *Wind Energy Explained, Theory, Design and Application.* Chichester, UK: John Wiley & Sons LTD; 2002.

3. Katsanos EI, Thöns S, Georgakis CT. Wind turbines and seismic hazard: a state-of-the-art review. *Wind Energy.* 2016;19:2113–2133.

4. Lombardi D, Bhattacharya S, Muir Wood D. Dynamic soil-structure interaction of monopile supported wind turbines in cohesive soil. *Soil Dyn Earthq Eng.* 2013;49:165–180.

5. Arany L, Bhattacharya S, Macdonald J, Hogan SJ. Simplified critical mudline bending moment spectra of offshore wind turbine support structures. *Wind Energy.* 2014;18:2171–2197.

6. Novak M. Dynamic stiffness and damping of piles. *Can Geotech J.* 1974;11:574–598.

7. Kaynia AM, Kausel E. Dynamics of piles and pile groups in layered soil media. *Soil Dyn Earthq Eng.* 1991;10:386–401.

8. Gerolymos N, Gazetas G. Phenomenological Model Applied to Inelastic Response of Soil-Pile Interaction Systems. *Soils Found.* 2005;45(4):119–132.

9. Sa'don NM, Pender MJ, Abdul Karim AR, Orense R. Pile Head Cyclic Lateral Loading of Single Pile. *Geotech Geol Eng.* 2014;32:1053–1064.

10. Prendergast LJ, Gavin K. A comparison of initial stiffness formulations for small-strain soil-pile dynamic Winkler modelling. *Soil Dyn Earthq Eng.* 2016;81:27–41.

11. Kaynia AM. *Dynamic Stiffness and Seismic Response of Pile Groups*: Massachusetts Institute of Technology; 1982.

12. Kourkoulis RS, Lekkakis PC, Gelagoti FM, Kaynia AM. Suction caisson foundations for offshore wind turbines subjected to wave and earthquake loading: effect of soil-foundation interface. *Géotechnique.* 2014;64(3):171–185.

13. Passon P, Kühn M. State-of-the-art and Development Needs of Simulation Codes for Offshore Wind Turbines. *University of Stuttgart.* 2005.

14. Zaaijer MB. Foundation modelling to assess dynamic behaviour of offshore wind turbines. *Appl Ocean Res.* 2006;28:45–57.

15. Winkler E. *Die Lehre von Elasticzitat und Festigkeit (On Elasticity and Fixity).* Prague, Czech Republic; 1867.

16. Bush E, Manuel L. Foundation Models for Offshore Wind Turbines Erica. In: 47th AIAA Aerospace Sciences Meeting Including The New Horizons Forum and Aerospace Exposition; 5–8 January, 2009; Orlando, Florida.

17. Klikvort RT. *Centrifuge modelling of drained lateral pile - soil response*; 2012. PhD thesis.

18. Boulanger RW, Curras CJ, Kutter BL, Wilson DW, Abghari A. Seismic soil-pile-structure interaction experiments and analyses. *J Geotech Geoenviron.* 1999;125:750–759.

19. Taciroglu E, Rha CS, Wallace JW. A Robust Macroelement Model for Soil-Pile Interaction under Cyclic Loads. *J Geotech Geoenviron.* 2006;132:1304–1314.

20. Schløer S. *Fatigue and extreme wave loads on bottom fixed offshore wind turbines. Effects from fully nonlinear wave forcing on the structural dynamics*; 2013. PhD thesis.

21. Damgaard M, Zania V, Andersen LV, Ibsen LB. Effects of soil-structure interaction on real time dynamic response of offshore wind turbines on monopiles. *Eng Struct.* 2014;75:388–401.

22. Zania V. Foundation Models for Offshore Wind Turbines Erica. In: Proceedings of the 9th International Conference on Structural Dynamics, EURODYN 2014; 30 June – 2 July, 2014; Porto, Portugal.

23. Novak M, Nogami T. Soil-pile interaction in horizontal vibration. *Earthq Eng Struct D.* 1977;5:263–281.

24. Kausel E. Early history of soil-structure interaction. *Soil Dyn Earthq Eng.* 2010;30:822–832.

25. Ziegler L, Voormeeren S, Schafhirt S, Muskulus M. Sensitivity of Wave Fatigue Loads on Offshore Wind Turbines under varying Site Conditions. *Enrgy Proced.* 2015;80:193–200.

26. Krathe VL, Kaynia AM. Implementation of a non-linear foundation model for soil-structure interaction analysis of offshore wind turbines in FAST. *Wind Energy.* 2017;20(4):695–712.

27. Jonkman J, Buhl MJ. *FAST user's guide*. Golden, Colorado; 2005.

28. Iwan VL. On a class of models for the yielding behavior of continuous and composite systems. *J Appl Mech.* 1967;34(3):612–617.

29. Aasen S, Page AM, Skau KS, Nygaard TA. Effect of foundation modelling on the fatigue lifetime of a monopile-based offshore wind turbine. *Wind Energy Sci.* 2017;2:361–376.

30. Bisoi S, Haldar S. Dynamic analysis of offshore wind turbine in clay considering soil-monopile-tower interaction. *Soil Dyn Earthq Eng.* 2017;63:19–35.

31. Carswell W, Johansson J, Løvholt F, Arwade AR, Madshus, DeGroot. Foundation damping and the dynamics of offshore wind turbine monopiles. *Renew Energ.* 2015;80:724–736.

32. ADINA. *ADINA R&D, Inc.* Watertown, Massachusetts; 2014.

33. NGI. *Description of INFIDEL - a non-linear, 3-D finite element program.* Oslo, Norway; 1991.

34. Andersen LV, Vahdatirad MJ, Sichani MT, Sørensen JD. Natural frequencies of wind turbines on monopile foundations in clayey soils - A probabilistic approach. *Comput Geotech.* 2012;43:1–11.

35. Bayat M, Andersen LV, Ibsen LB. p-y-$\dot{y}$ curves for dynamic analysis of offshore wind turbine monopile foundations. *Soil Dyn Earthq Eng.* 2016;90:38–51.

36. Markou AA, Manolis GD. Mechanical models for shear behavior in high damping rubber bearings. *Soil Dyn Earthq Eng.* 2016;90:221–226.

37. Markou AA, Manolis GD. Mechanical formulations for bilinear and trilinear hysteretic models used in base isolators. *B Earthq Eng.* 2016;14(12):3591–3611.

38. Naeim F, Kelly JM. *Design of Seismic Isolated Structures: From Theory to Practice.* New York, USA: John Wiley & Sons; 1999.

39. Vucetic M, Dobry R. Effect of soil plasticity on cyclic response. *Geotech Geol Eng.* 1991;117:89-107.

40. American Petroleum Institute (API). *Recommended practice 2a-wsd planning, designing, and constructing fixed offshore platforms*; 2014.

41. Reese LC, Matlock H. Non-dimensional solutions for laterally loaded piles with soil modulus assumed proportional to depth. In: Proceedings of the 8th conference on soil mechanics; 14 – 15 September, 1956:1–41.

42. McClelland B, Focht JA. Soil modulus for laterally loaded piles. *J Soil Mech Found Div. In: Proceedings of the American society of civil engineers.* 1958:1–22.

43. Lombardi D, Bhattacharya S, Muir Wood D. Dynamic soil-structure interaction of monopile supported wind turbines in cohesive soil. *Soil Dyn Earthq Eng.* 2013;49:165–180.

44. Jung S, Kim SR, Patil A, Hung LC. Effect of monopile foundation modeling on the structural response of a 5-MW offshore wind turbine tower. *Ocean Eng.* 2015;109:479–488.

45. Cui L, Bhattacharya S. Soil-monopile interactions for offshore wind turbines. *P I Civil Eng - Eng Comput Mech.* 2016;169(4):171–182.

46. Jonkman J, Butterfield S, Musial W, Scott G. *Definition of a 5-MW Reference Wind Turbine for Offshore System Development*: National Renewable Energy Laboratory; 2009.

47. Besson J, Cailletaud G, Chaboche JL, Forest S. *Non-Linear Mechanics of Materials.* Dordrecht, Netherlands: Springer; 2010. ISBN 978-90-481-3355-0.

48. Chopra AK. *Dynamics of structures, Theory and Applications to Earthquake Engineering.* Boston: Prentice Hall; 2012. 4^{th} edition.

49. Bhattacharya S. Challenges in Design of Foundations for Offshore Wind Turbines. *IET - Eng Tech Ref.* 2014, DOI doi: 10.1049/etr.2014.0041.

$\square$